

We are IntechOpen, the world's leading publisher of Open Access books Built by scientists, for scientists

6,100

Open access books available

149,000

International authors and editors

185M

Downloads

Our authors are among the

154

Countries delivered to

TOP 1%

most cited scientists

12.2%

Contributors from top 500 universities



WEB OF SCIENCE™

Selection of our books indexed in the Book Citation Index
in Web of Science™ Core Collection (BKCI)

Interested in publishing with us?
Contact book.department@intechopen.com

Numbers displayed above are based on latest data collected.
For more information visit www.intechopen.com



Applications of Metamaterials and Metasurfaces

Babar Kamal, Usman Ali, Jingdong Chen and Sadiq Ullah

Abstract

Metamaterials are efficiently homogenizable arrangements of artificial structural components engineered to achieve beneficial and exotic electromagnetic (EM) properties not found in natural materials. Metasurfaces are the two-dimensional analogue of metamaterials consisting of single-layer or multi-layer stacks of planar structures. Both metamaterials and metasurfaces have great potential to be used in a wide range of applications, e.g., antennas, polarization converters, radar cross section (RCS) reduction, and absorbers, to control the amplitude, phase and polarization of the reflected and transmitted EM waves. This chapter presents a brief overview of the known types and applications of metamaterials/metamaterials followed by comprehensive analysis of these surfaces for antennas performance enhancement, polarization conversion, RCS reduction, and wave absorption.

Keywords: metasurface, electromagnetic waves, antennas, polarization, absorption

1. Introduction

Metamaterials are artificial three dimensional (3D) structures composed of periodic subwavelength metal/dielectric arrangement of unit cells with exact dimensions [1]. A metamaterial is volumetric and is intended to provide artificial permeability (μ) and permittivity (ϵ) with extremely powerful electromagnetic (EM) wave control capabilities [2], leading to exceptional EM properties, which are often provided via resonant effects managed by the geometry of the unit cells [3]. Metamaterials have been used in such applications as magnetic resonance imaging [4], sensors [5], and antenna systems (for gain enhancement and beam steering) [6]. For EM integration, bulky sizes, low efficiencies, complex fabrication process are some of the disadvantages of metamaterials. To overcome these disadvantages, the two-dimensional (2D) metamaterials, which are known as metasurfaces, have been developed. They have attracted increasing research and development over recent years due to their small size, larger bandwidth, high efficiency, ease of fabrication, and less lossy characteristics [7–9]. A metasurface (MS) is intended to manipulate the amplitude, phase, and polarization of incident EM waves. Traditional techniques achieve polarization control of EM waves through using the crystal optical activity and Faraday effect. The drawback associated with these techniques are narrow bandwidth and incident angle response, and the resulting devices are large in size [10]. Similarly, the conventional

absorbers, which are used to achieve absorption of EM waves, are bulky, fragile and challenging to manufacture. Metasurfaces can be utilized to control the EM waves within one thin layer, leading to substantial advantages, such as low cost, and high degree of integration. They can be used in a wide spectrum of applications such as perfect lens [11], perfect absorbing [12], invisibility [13], light bending [14], and polarization conversion [15], to name but a few.

In this chapter, various metamaterials are discussed for antenna systems to achieve high gain as well as wide bandwidth, size reduction and reduced Specific Absorption Rate (SAR). Also discussed are metasurfaces with unique geometrical arrangements to achieve polarization conversion, RCS reduction, and absorption of EM waves. The basic design requirements, fundamental principle, working mechanism, parametric extraction and unit cell configurations are discussed in detail to explain the core concept of metamaterials/metasurfaces.

2. Applications of metamaterials

2.1 Metamaterials in the design of antenna

The metamaterials have unique physical characteristics that are not found in nature but are highly desirable for use in many applications including but not limited to invisible submarines, microwave invisibility cloaks, compact effective antennas, and negative refractive-index lenses [16]. One of the most important applications of metamaterials is in antenna design [17]. Due to the distinctive characteristics of metamaterials, novel antennas can be designed that are not possible with the materials found in nature. The metamaterial integrated in antennas, which consist of a single layer or double layers, can either serve as substrates or be added to the geometry of the antenna to improve the overall performance of the antenna [18, 19]. Scientific investigations showed that introducing metamaterials into the antenna design can improve several important parameters and decrease the overall volume of the antenna while increasing the radiated power and improving gain and directivity [20, 21]. Moreover, these materials can be integrated into antennas to reduce the side and back lobe radiation as well as to restrict the specific absorption rate (SAR) in scenarios where they are worn on the body [22, 23]. Depending on how the antenna is designed, different construction and applications of these materials can be used.

2.1.1 Metamaterial unit cell

The metamaterials used in antennas can be of a single unit cell or an array of unit cells. Therefore, the most crucial step in creating the metamaterials is the design of the unit cell. Its key features that affect the permittivity (ϵ), permeability (μ) and resonance frequency (f_r) must be considered and analyzed [24], based on which as well as the requirements at the desired frequencies, various parameters, e.g., the size and shape of the unit cell, its ϵ , μ , and resonant frequencies are obtained. To satisfy the given requirements at the resonant frequency, the dimensions and type of unit cell are optimized [25]. The unit cell size may vary greatly depending on the geometry of the metamaterials, but it is generally less than one-tenth of the working wavelength [26], as depicted in **Figure 1**.

For instance, several metamaterial unit cells at the 2.4 GHz Industrial Scientific and Medicinal (ISM) frequency band are designed and simulated using the procedures

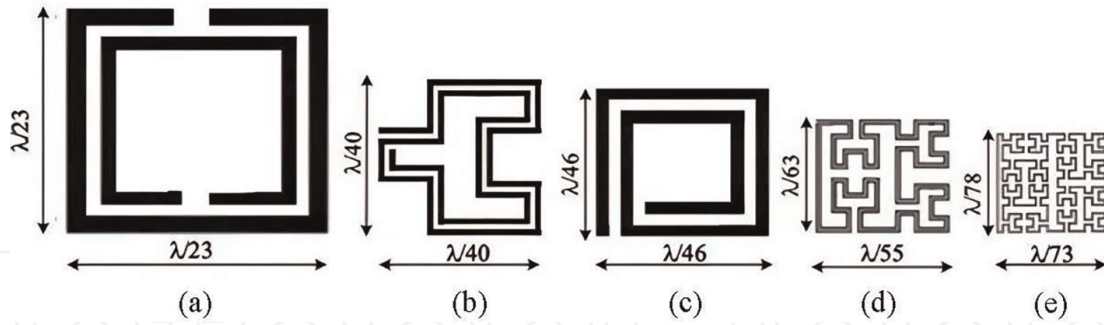


Figure 1. Layout of a unit cell of an addition with square ring resonator (SRR) (a), the addition of a 2nd order Hilbert fractal (b), a square spiral (c), the addition of a 3rd order Hilbert fractal (d), the addition of a 4th order Hilbert fractal inclusion (e) with the increase of order the size is reduced [26].

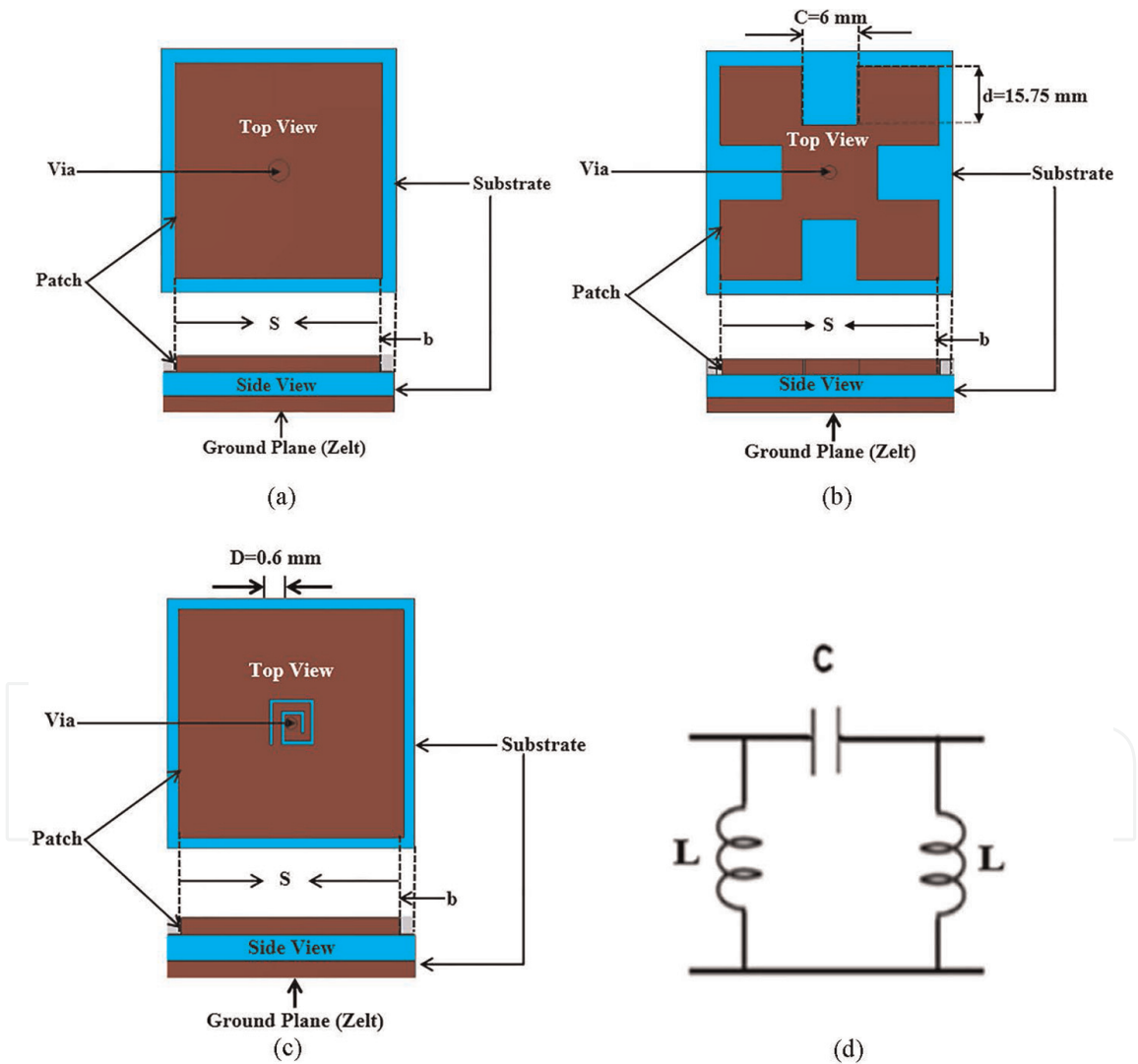


Figure 2. Geometry of: (a) the mushroom-like structure, (b) the Slotted structure, (c) the Spiral structure. (d) The LC-resonant circuit of the unit cell [23].

listed below. To meet the homogeneous requirements by metamaterials, it is critical that the size of the unit cell needs to be smaller than the guided wavelength (Figure 2).

Figure 2 illustrates the geometry of the different unit cells. These structures function as an LC parallel resonant circuit. The capacitance C and inductance L , whose value depends on the unit cell's geometry and size [27], determine the in-phase bandwidth and resonant frequency.

The capacitance is due to the fringing between adjacent unit cells. It can be calculated as:

$$C = \frac{w\epsilon_0(1+\epsilon_r)}{\pi} \cosh^{-1} \frac{(w+g)}{g} \quad (1)$$

where w , g and ϵ_0 represent the width of the unit cell, the gap between the neighboring unit cells, and the dielectric constant of free space, respectively. The following relationship can be used to calculate the inductance L , which is directly related to the substrate's thickness or the length of the metal via.

$$L = \mu_0\mu_r t \quad (2)$$

The optimized unit cells dimensions at the desired 2.4 GHz frequency is shown in **Figure 2**. The dimensions are: $w = 0.323\lambda_{2.4 \text{ GHz}}$, $g = 0.018\lambda_{2.4 \text{ GHz}}$, where $\lambda_{2.4 \text{ GHz}}$ is the free space wavelength at 2.4 GHz, $\text{via (radius)} = 0.004\lambda_{2.4 \text{ GHz}}$. The mentioned surfaces are categorized for surface wave suppression and in-phase reflection characteristics. The unit cell's resonance frequency is then given as:

$$f_r = \frac{1}{2\pi\sqrt{LC}} \quad (3)$$

2.1.2 In-phase reflection

The simulation setup and boundary conditions for in-phase reflection analysis of the three metamaterial structures are shown in **Figure 3**. Linearly polarized (TE₁₀) plane waves are used to excite these surfaces. The in-phase reflection (0°) at the resonant frequency of 2.4 GHz is determined by the three unit cells (**Figure 4**). The

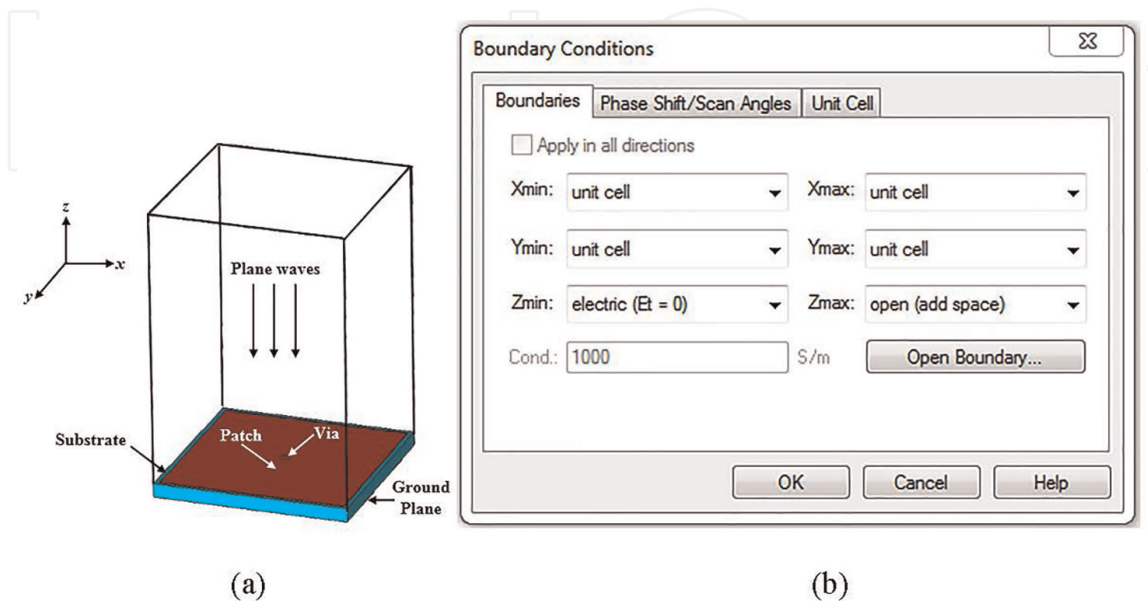
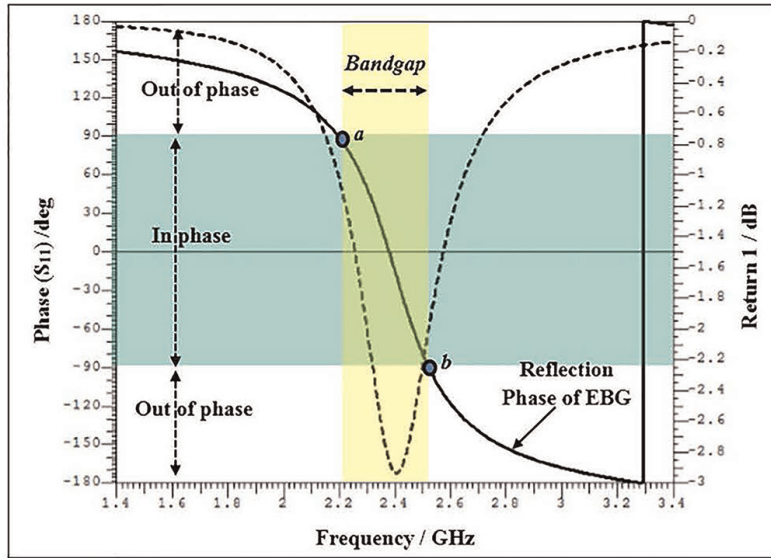
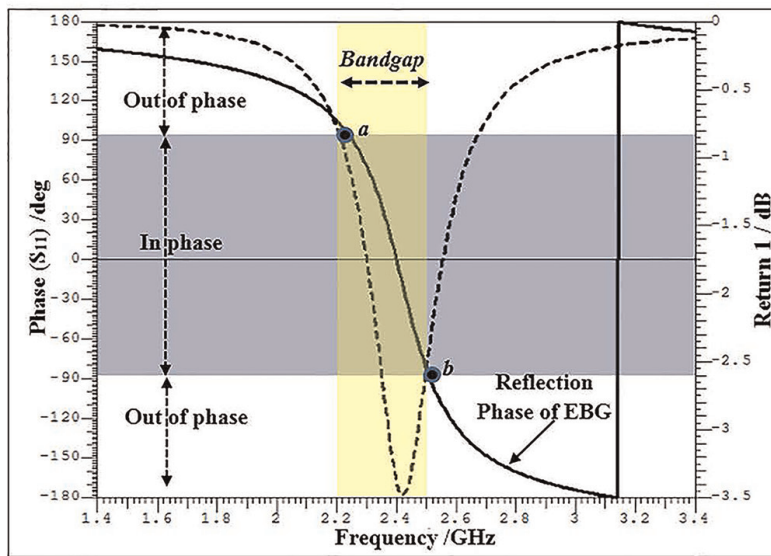


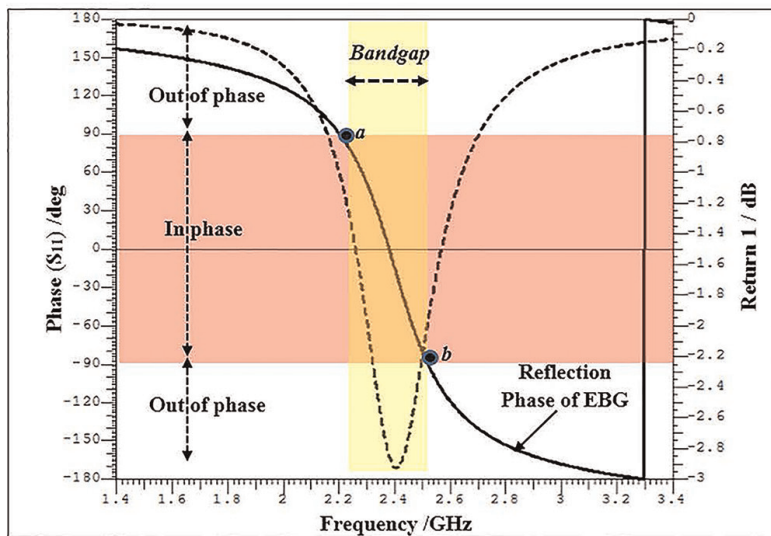
Figure 3. Simulation setup of the unit cell for the in-phase reflection analysis [23].



(a)



(b)



(c)

Figure 4. Reflection phase characteristics of three structures: (a) Mushroom-like, (b) Slotted, and (c) Spiral [23].

surface acts like a perfect magnetic conductor (PMC) at this frequency [23]. At a lower frequency of 1.4 GHz and a higher frequency of 3.4 GHz, the reflection phase is $+180^\circ$ and -180° . At these two frequencies, the surface acts like a perfect electric conductor (PEC). The reflection phase changes from $+90^\circ$ to -90° at points “a” and “b”, respectively, crossing 0 at the central frequency of 2.4 GHz. In the given reflection bandwidth, the metamaterial acts like an artificial magnetic conductor (AMC). The reflection phase bandwidth, denoted as BW_{rp} , can be calculated as follows:

$$BW_{rp} = \frac{f_b - f_a}{f_c} \times 100, \quad (4)$$

where f_b , f_a , and f_c denote, respectively, the higher, lower, and central frequencies.

2.1.3 Surface wave bandgap

To analyze the surface wave bandgap characteristics, a 50- Ω suspended microstrip line at a distance of 1.5 millimeters above the array of unit cells is used (**Figure 5**). To examine the transmission coefficient of the metasurface, the microstrip line is powered using a waveguide port at both ends. Note that the dispersion diagram method can also be used to study the bandgap characteristics.

The S_{12} and S_{11} of the aforementioned three metasurface structures are plotted in **Figure 6**. It is found that the magnitude of the S_{12} directly influences the surface wave suppression. If setting the required wave suppression threshold of S_{12} to -20 dB, the mushroom-like structure efficiently suppresses the surface waves in the frequency band from 2.34 to 2.57 GHz according to **Figure 6**. Consequently, this type of structure provides both in-phase reflection and surface wave suppression characteristics at the resonant frequency. This surface functions as a standard PEC ground plane outside of the 2.34–2.57 GHz frequency band. According to the pre-defined criteria in this band, the remaining two metamaterial structures, i.e., the spiral and the slotted, exhibit in-phase reflection characteristics only at 2.4 GHz but without sufficient surface wave suppression. The surface wave bandgap of the spiral metasurface shifts slightly to the left of the 2.4 GHz point as a result of the inductive loading of this surface. CST Microwave Studio software [23] is used to study and calculate the unit cell's properties, which show that the unit cell clearly serves as an AMC.

Similarly, a dual band metasurface unit cell is considered and examined using the following steps. The layered structure is shown in **Figure 7**. The dual-band unit cell consists of three layers. A square dielectric block has been placed between the first and

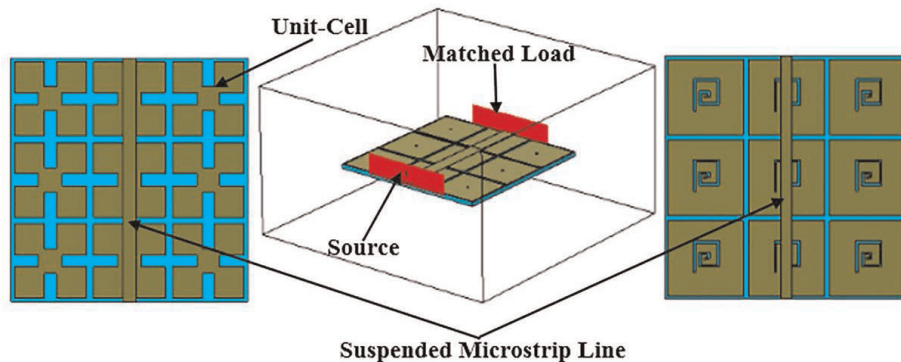


Figure 5. Simulation setup for the surface wave bandgap characterization [23].

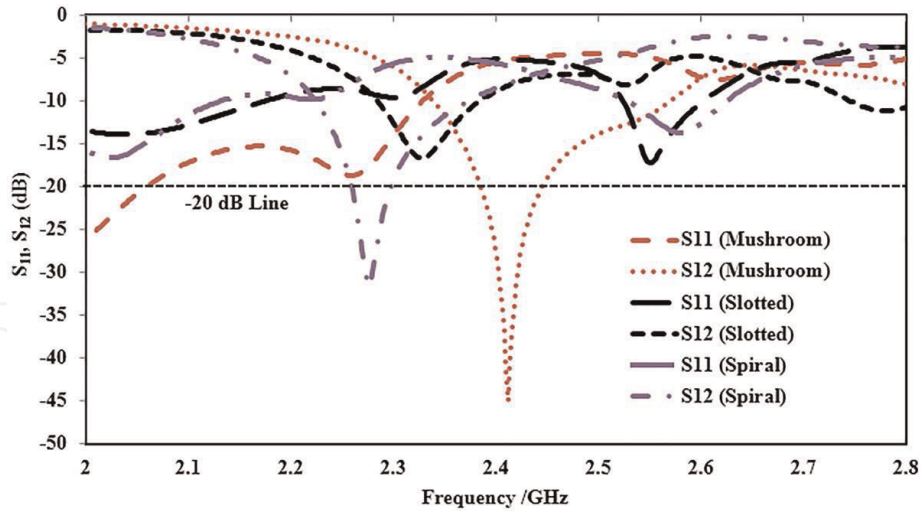


Figure 6. S_{11} and S_{12} characteristics of three metamaterial structures [23].

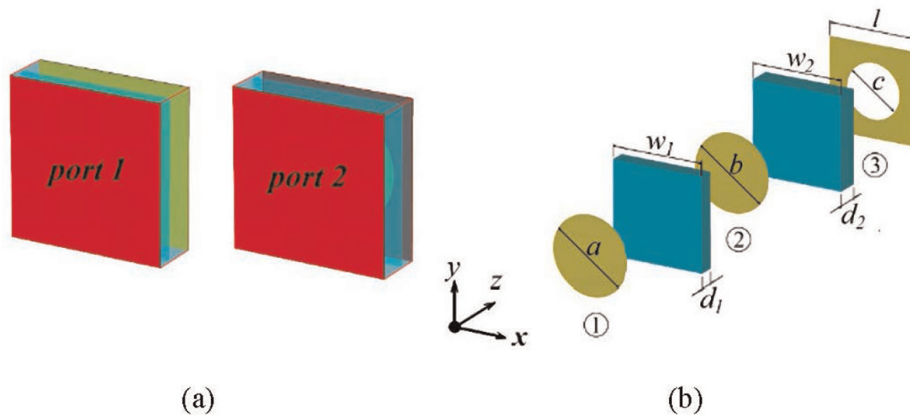


Figure 7. (a) Layout of the Unit Cell from ports 1 to 2. (b) Hierarchical diagram of EM incidence waves [28].

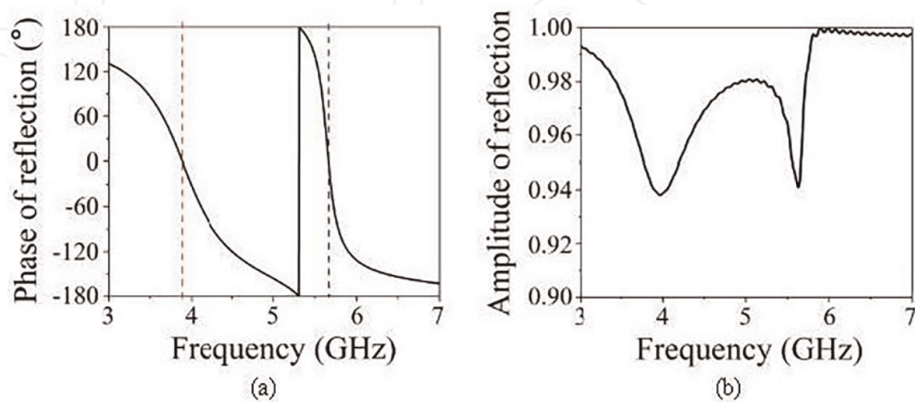


Figure 8. Simulated results for a unit cell: (a) phase of the reflection coefficient, and (b) amplitude of the reflection coefficient [28].

second layers, which are made up of circular metal patches with diameters of a and b , respectively. The third layer consists of a square metal patch with a central circular slot. Between the second and third layers, a square dielectric block is inserted [28].

The magnetic and electric wall boundary conditions were forced along the $\pm x$ and $\pm y$ directions to produce a waveguide. Then, the circular metal patch's surface received port 1 of the waveguide and its reference plane, and the square metal patch's surface received port 2 of the waveguide with the circular slot. Due to the linear polarization along the y -direction, excitation of port 1 is comparable to a plane wave incident along the z -direction. **Figure 8(a)** shows the unit cell during its reflection phase. Phase is zero at 3.89 and 5.66 GHz. At these two frequencies, the unit cell is equivalent to mu-negative metamaterials (MNMs). **Figure 8(b)** shows that at these two operating frequencies, the reflection coefficient is approximately 0.94, which demonstrates the partial reflection property of the unit cell.

3. Metamaterials in antennas engineering

In this section, the application of metamaterials for enhancing antenna parameters is presented and explained. Antennas play an important role on wireless communication while materials play a crucial role on the antenna performance. The widely used microwave and radio frequency substrate materials in antenna applications include artificial magnetic conductors (AMCs) and high-impedance surfaces (HISs). HISs or AMCs are used to build small, low-profile antenna systems by placing them close to or all around the antenna radiating elements. Metamaterials can also be used to build the antenna or as part of the feeding mechanism for the antenna system.

What discussed in this section includes gain and directivity enhancement, bandwidth enhancement, surface wave suppression and SAR reduction of the antenna when placed in close proximity to the human body, and miniaturization of microstrip antennas by loading the materials as a patch, mounting them as a superstrate above the main radiator, placed them at the ground plane, or embedding them in the substrate. These surfaces are used in antennas to solve a variety of problems, thereby circumventing the limits of the antennas designed with the conventional approaches. For example, placing the material above the reflector can help enhance the radiation properties of the antenna, reduce the backward radiation and redirect the radiation in the forward direction [29]. The electromagnetic band gap (EBG) structure, first proposed by Sievenpiper in 1999 [30], was a mushroom-shaped structure with a ground plane loaded with a grid of square patches attached to the ground plane by a metallic through (**Figure 9**).

3.1 Incorporating metamaterial into antenna design

By incorporating metamaterial structures into the design of antennas, it is possible to decrease the antenna size, increase its gain and directivity, expand the bandwidth, and reduce side and back radiation. Metamaterial structures can also be used to create multiband applications. This section focuses on explaining the benefits of incorporating metamaterial structures into the antenna design.

3.1.1 Gain enhancement

The performance degradation in gain, directivity, and efficiency is the fundamental disadvantage of small planar antennas. In the case of multiband applications, this issue becomes more severe, particularly in the lower frequency bands. To meet the requirements for the total link budget of the transceiver systems, antennas must

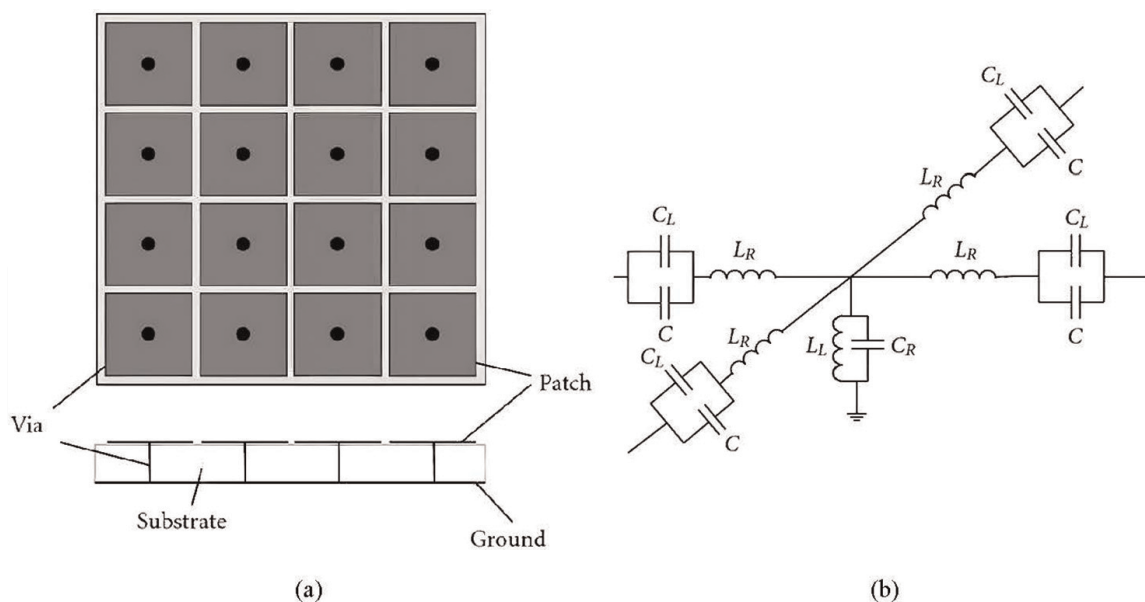


Figure 9. (a) Layout of the mushroom electromagnetic band gap (EBG) unit cell, (b) equivalent circuit model of the unit cell [31].

overcome the problem of low gain and efficiency. Besides using array antennas, metasurface antennas were recently introduced as an alternative candidate for various communication bands to improve the overall performance of the antenna by incorporating metamaterial structures (either AMM or AMC) into antenna designs.

Metamaterial are integrated into the antenna by either arranging their unit cells in such a way that they surround the antenna radiating element [23, 32], or using them as a ground plane loading or etching of the antenna, in which AMC functions as a zero-degree reflection for the incident waves at the antenna working frequency [33–36]. There are different ways to use metamaterial structures for enhancing the antenna gain, as illustrated in **Figure 10**. However, regardless of what method is used, the unit cell type, the number of superstrates used, and the distance between the primary radiating elements and the superstrate all play an important role on the gain improvement. The unit cells can be arranged in different ways, e.g., surrounded by the radiating elements of the antenna or loaded on both or one side of the substrate. In order for the metamaterial to have unique physical properties that fit the resonance frequency of the antenna, the size of the unit cells needs to be properly designed. Due to their negative permeability characteristics, the unit cells can be simply integrated with radiating components and used as insulators to reflect surface waves. The traditional antenna's gain can be improved by adding metamaterial unit cells around it [37]. The two key determinants that affect the gain attained are the resonant frequency of the desired antenna and the number of unit cells used. The array of unit cells with various relative permittivity is loaded away from the primary radiating element in the case of metamaterial superstrates. These unit cells can be loaded on either side of the superstrate. The number of superstrates, the number of unit cells, and the distance between the radiating element and the superstrate all play a key role on the gain performance and directivity of the conventional antenna [38] (**Figure 11**). The directivity and gain of the traditional antenna can be significantly increases by integrating metamaterial into the antenna design. However, the overall size and thickness of the antenna are also increased.

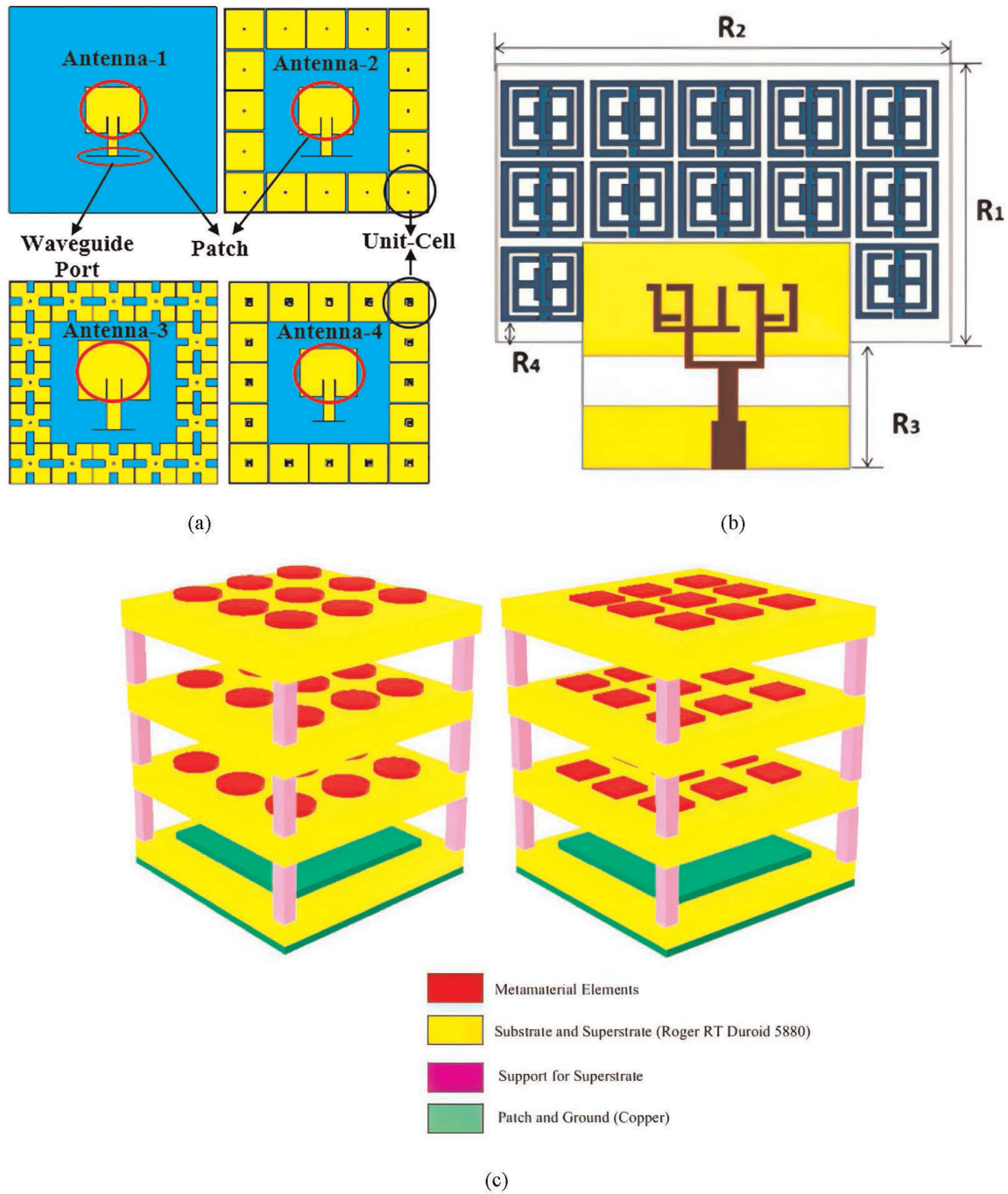


Figure 10. Application of metamaterials to improve the antenna gain, including: (a) radiating element surrounded by unit cells, (b) antenna loading with metamaterials, and (c) metamaterial as a superstrate [23, 33, 34].

3.1.2 Metamaterials for bandwidth enhancement

In addition to improving the gain and directivity of conventional antennas, metamaterials can also be used to increase the impedance bandwidth of the antennas. To increase the bandwidth, the metasurfaces can be utilized as part of the antenna or can be used as a superstrate placing over the main radiating element, as was discussed for increasing the gain of the antenna (**Figure 11**). The superstrate can be placed above or below the metamaterial unit cells. The number of unit cells used and the distance between the radiating element and the superstrate have a great impact on the antenna impedance bandwidth. The configuration of the antenna with superstrate material and

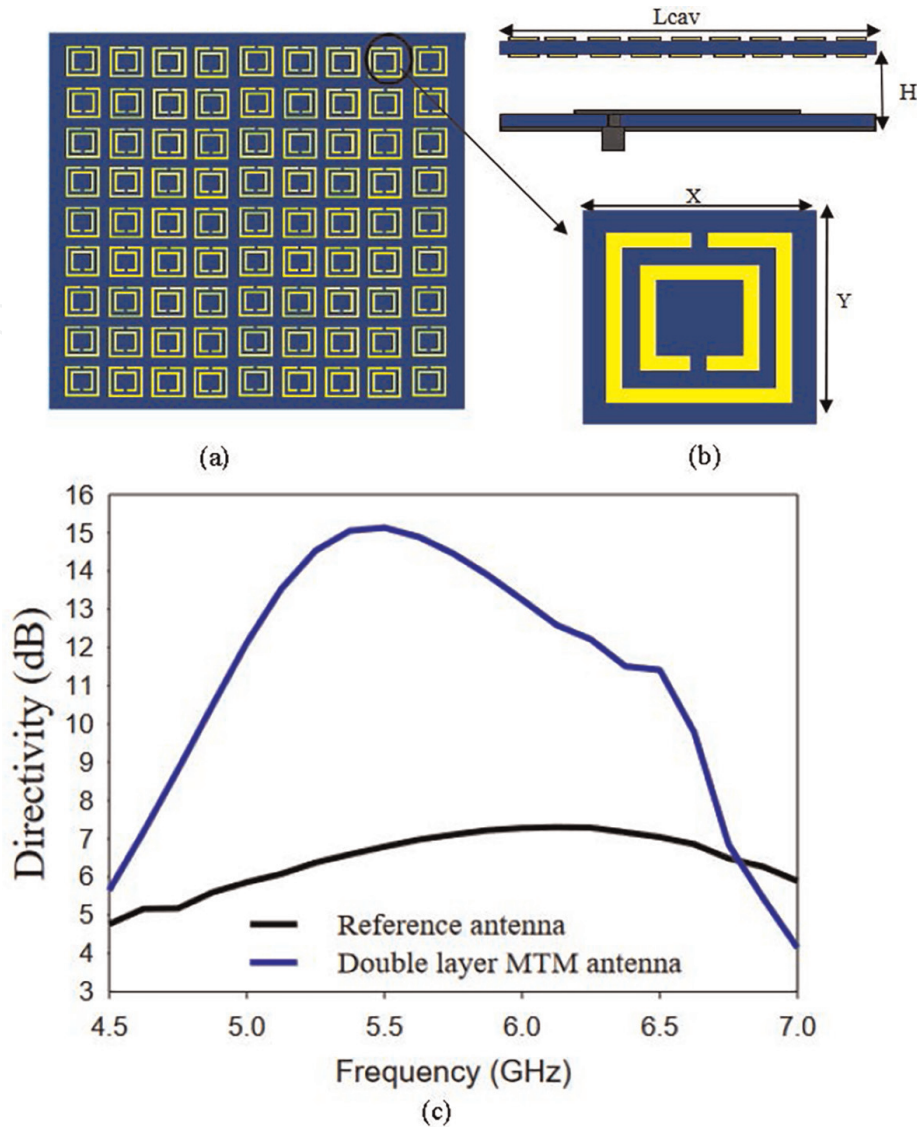


Figure 11. Patch antenna with a double layer metamaterial superstrate: (a) front and top view of the antenna, (b) unit cell of SRR, and (c) directivity with/without superstrate [38].

the simulation of the reflection coefficient with and without the metamaterial are shown in (Figure 12). The bandwidth for the higher frequency band is significantly increased by the antenna integrated with metamaterial, from only 9.35–28%. Moreover, the third band has increased to 27.81% and moved slightly higher in frequency. Incorporating the metamaterial unit cells also matches the lower band [39].

3.1.3 Metamaterials for antenna size reduction

To reduce the antenna size, numerous design strategies are proposed, including shorting pins, generating disturbances, employing high dielectric substrate materials, fracturing the shape, etc. Many antenna designers have recently utilized metamaterial structures as defective ground structures (DGS) for small antennas. Using these structures as a DGS can produce unusual characteristics at the resonance frequency of the antenna. In this instance, the unit cell size is the same as the size of the DGS's removed portion [40, 41]. Figure 13 depicts the geometry of the antenna and the metamaterial loaded with the bottom layer. The simulated S_{11} of the antenna with and

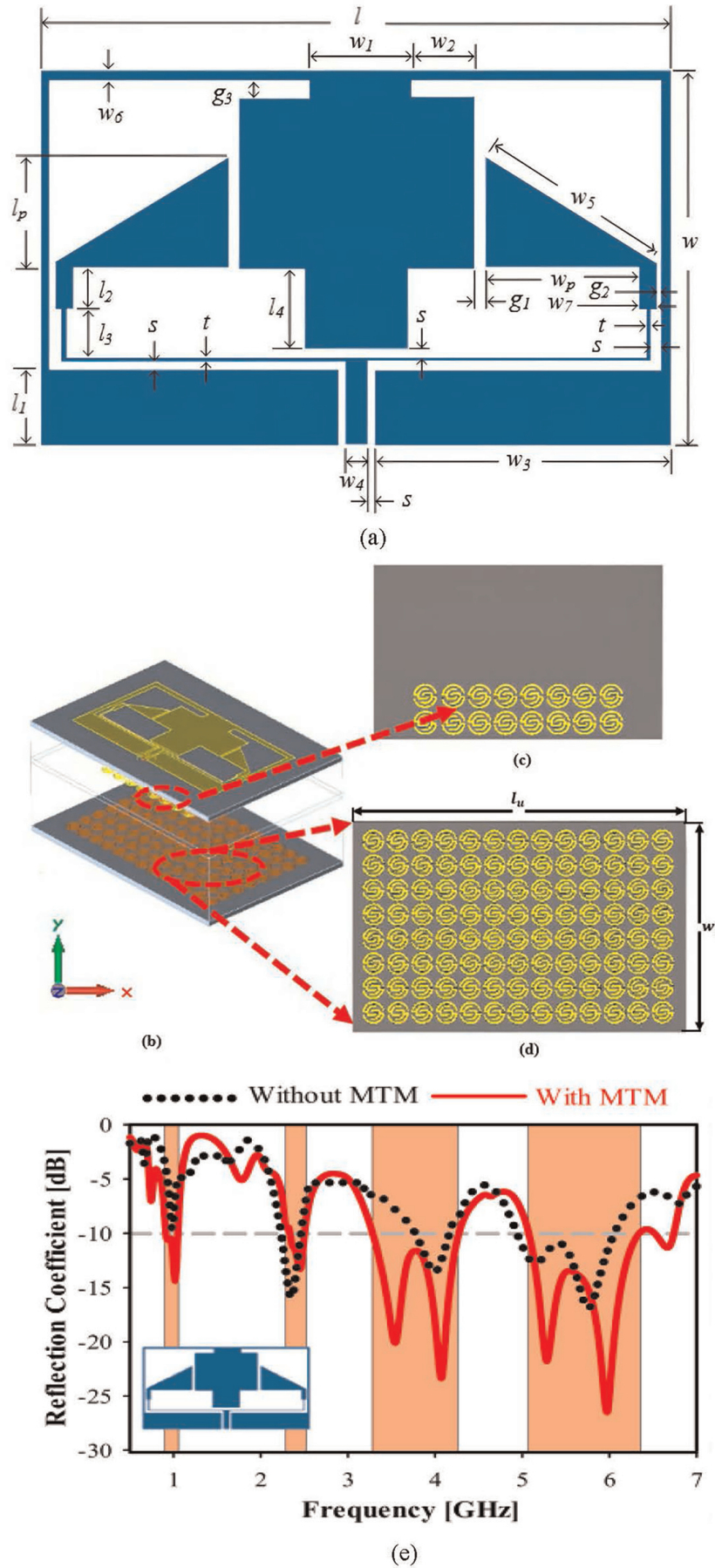


Figure 12. Layout of the antenna (a) front view, (b) 3D view, (c) back view, (d) a suspended separator MMT layer, (e) S_{11} with and without metamaterial [39].

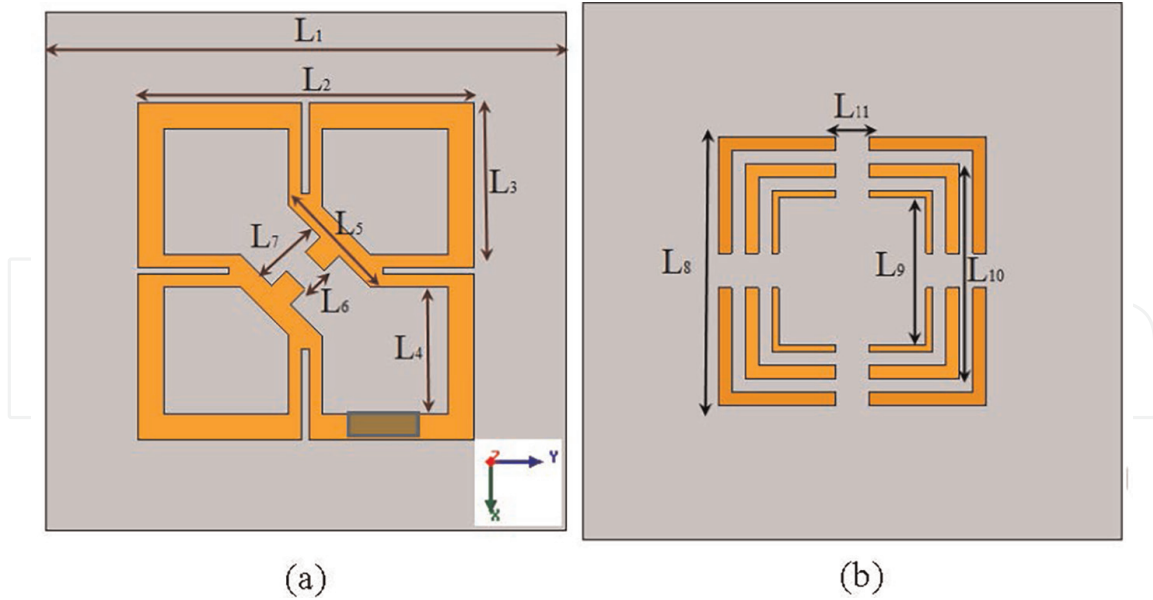


Figure 13.
 Geometry of the antenna: (a) top view, and (b) MMT load at the bottom layer [41].

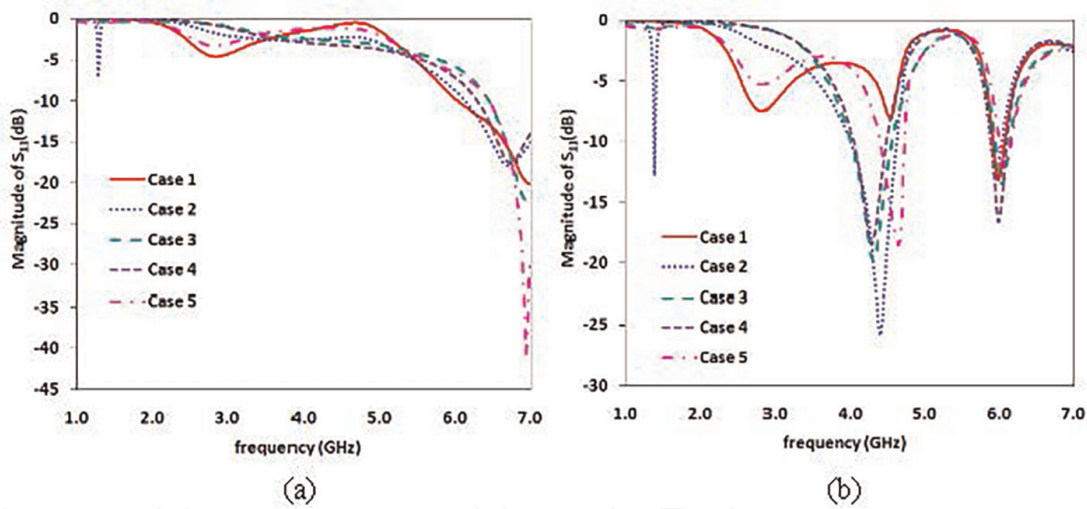


Figure 14.
 Reflection coefficient (S_{11}): (a) without metamaterial, and (b) with metamaterial [41].

without metamaterial is presented in **Figure 14**. The S_{11} shows that the proposed antenna operates at 7 GHz (**Figure 14**). But when a metamaterial layer of multi parallel rings are added, the resonance frequency is shifted from 7 GHz to 4 GHz and the size of the antenna is considerably reduced.

3.1.4 Metamaterials for the reduction of specific absorption rate

Wireless body area networks (WBAN) are widely employed in many different applications, including mobile communication, military applications, medical diagnosis, and rescue services. In these kinds of applications, the antennas must be operated in close contact to the human body. The backward radiation is absorbed into human body tissues as a result of its near vicinity to the human body and may seriously harm these tissues. The absorption of energy by human body tissue is defined by the specific absorption rate (SAR) [42]. The SAR is defined as the rate of electromagnetic energy

absorbed by the human body tissue per unit mass. The safe limit of the SAR for mobile phones and similar electronic gadgets has been defined by international standards. The US standard defines the safe limit for SAR as 1.6 W/kg average over 1 g of tissue, while the EU defined it as 2.0 W/kg average over 10 g of tissue [27, 43]. The SAR must comply with the safe limits established by international bodies in order to protect the human body from harmful radiation.

Several techniques, including the use of reflectors [44], RF shielding with ferrite and conductive materials [45], and the use of highly directional antennas [46], have been utilized to reduce SAR. Recently, metamaterials like AMC, SRR, and EBG are investigated to block electromagnetic waves towards the human body and to reduce SAR [47–49]. **Figure 15** shows the design and simulation setup of the proposed antennas with polarization dependent metamaterial and a high effective medium ratio [50]. The SAR of the mobile phone without metamaterial structure is calculated and analyzed using L, S, and C-band frequencies, considering both 1 and 10 g of tissues. In this case, the metamaterial structure acts as a shielding material and protects the human head from harmful radiation. It is evident that the unique metamaterial structure lowers the SAR value emitted from a mobile phone by 98%. Likewise, a metamaterial based fabric antenna at ISM band is shown in **Figure 16**, where the metamaterial structure behaves as EBG/AMC [51]. The proposed antenna is analyzed for SAR with and without metamaterial structures.

The SAR analysis of the traditional and the antenna integrated with metamaterial at the ISM band considering the Federal Communications Commission (FCC) standard of 1 g of human body tissue is presented in **Figure 17**. It is observed that the traditional antenna, when placed in the vicinity of human body, gives a SAR of 7.78 W/kg, exceeding the safe limit. However, the antenna integrated with metamaterial when placed in close contact with the human body gives an SAR value of 0.028 W/kg, which is within the safer limit of the FCC standard of 1.6 W/kg averaged

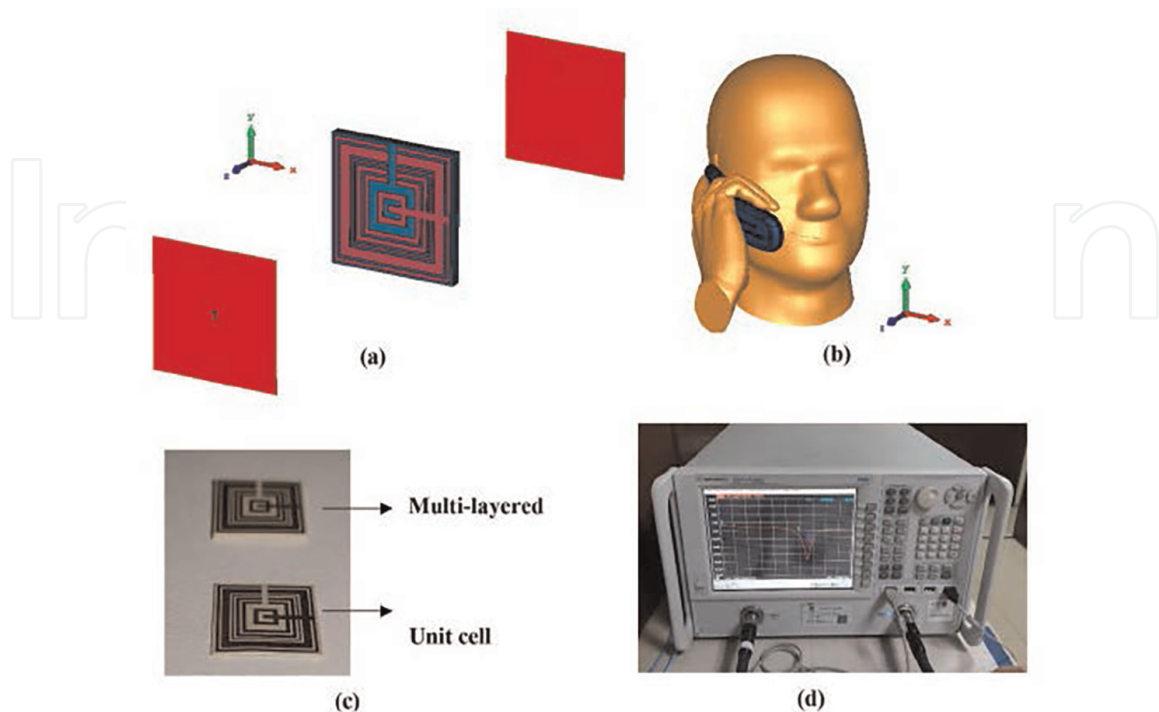


Figure 15. Layout and simulation setup: (a) metamaterial structure, (b) Voxel model (human head and hand), (c) Fabricated metamaterial structure, (d) Agilent N5227A VNA [50].

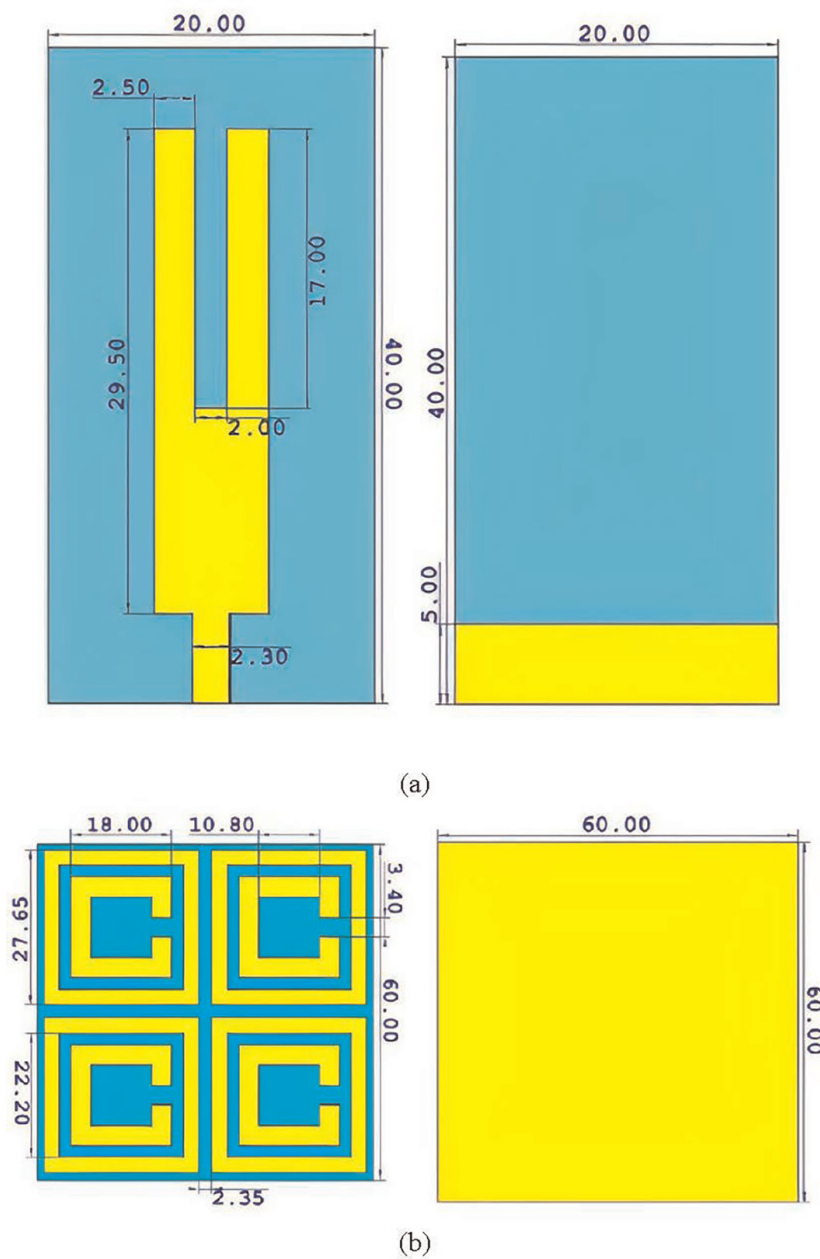


Figure 16. Design layout for: (a) U-shaped fabric antenna, and (b) Metamaterial on fabric material [51].

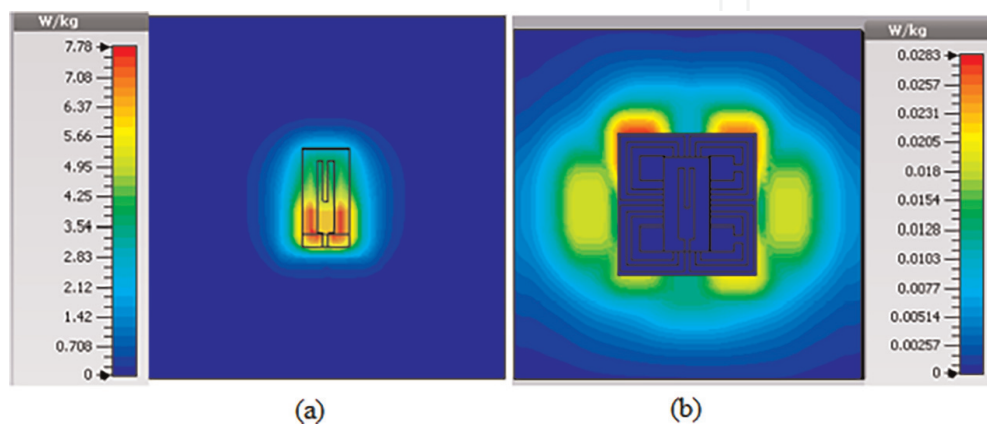


Figure 17. Simulated SAR of the proposed U-shaped antenna (a) without metamaterial, and (b) with metamaterial [51].

over 1 g of tissue. Hence, the metamaterial integrated antenna play a vital role to reduce the SAR significantly compared to its conventional counterpart.

4. Applications of metasurfaces

4.1 Metasurfaces for polarization conversion

Polarization is the characteristic of a wave's oscillation, i.e., having a particular direction relative to the wave's propagation. The polarization of an EM wave is defined as the direction of the electric field oscillation in a plane transverse to the propagation. The process of altering the polarization state of a wave after reflecting, transmitting from a medium is known as polarization conversion. Wave plates, also known as retarders, modify the polarization state by retarding (or delaying) one component of polarization with respect to its orthogonal component. Wave plates alter the polarization state of EM waves. The most common types of wave plates include the half-wave plates and quarter-wave plates. The former changes the path of linearly polarized EM waves, while the latter transforms linearly polarized EM waves to circular polarized one, and vice versa. Every polarization state can be decomposed into orthogonal components, and the phase difference between them must be regulated in order to convert one polarization to another. Metasurface structures with asymmetric resonators having low co-polarization reflection and high cross-polarization reflection are usually used for polarization conversion. In the following subsections, the mathematical background and designs examples of the polarization converting metasurfaces will be discussed.

4.1.1 Polarization converting metasurface

Polarization converting metasurface (PCMS) is a device that transforms the polarization state of an incident EM wave with no significant loss. When an incident EM wave is transformed from y -polarized to x -polarized wave upon reflection from the metasurface, the corresponding conversion is called cross polarization conversion. Generally, the reflection coefficient is defined as a ratio of reflected field E^{ref} and incident field E^{inc} , (i.e., $r = E^{\text{ref}}/E^{\text{inc}}$). The electric field is a plane wave propagating along the z -direction and is given as:

$$E = \hat{u}^{\text{pol}} E_o e^{-j(kz-t)} \quad (5)$$

where \hat{u}^{pol} , E_o , k , and ω , represents, respectively, the polarization direction, amplitude of electric field, wave number, and the angular frequency. The correlation among the incident and reflected electric fields of LP incidence wave oriented along $(x-y)$ -direction is given by the Jones matrix [52]:

$$\begin{bmatrix} E_x^{\text{ref}} \\ E_y^{\text{ref}} \end{bmatrix} = \begin{bmatrix} R_{xx} & R_{xy} \\ R_{yx} & R_{yy} \end{bmatrix} \begin{bmatrix} E_x^{\text{inc}} \\ E_y^{\text{inc}} \end{bmatrix} \quad (6)$$

where R_{xx} and R_{yy} represents co-polarized reflection and are defined as $R_{xx} = E_x^{\text{ref}}/E_x^{\text{inc}}$, $R_{yy} = E_y^{\text{ref}}/E_y^{\text{inc}}$, similarly R_{yx} and R_{xy} represents cross-polarized reflection and are defined as $R_{yx} = E_y^{\text{ref}}/E_x^{\text{inc}}$, $R_{xy} = E_x^{\text{ref}}/E_y^{\text{inc}}$. E_x^{inc} , E_x^{ref} is the incident and reflected x -polarized electric field and vice versa, respectively.

For efficient cross polarization transformation, the level of the cross-polarized reflection coefficients should be larger than -3 dB, i.e., $|R_{yx}|, |R_{xy}| > -3$ dB while the level of co-polarized reflection coefficient should be smaller than -10 dB, i.e., $|R_{xx}|, |R_{yy}| < -10$ dB [52]. To illustrate how polarization transformation is achieved, a metasurface composed of an arrow shaped resonator is designed as shown in **Figure 18(a)**. It is seen from the results shown in **Figure 19(a)** that the proposed PCMS fulfilled the aforementioned criteria and performs cross polarization conversion (CPC) in an ultra-wideband (10.1–26.0 GHz). Polarization conversion ratio (PCR) is usually expressed as the ratio of the power reflected in the cross-polarized component to the total reflected power, i.e., [53]:

$$\text{PCR} = \frac{|R_{yx}^2|}{|R_{yx}^2| + |R_{xx}^2|}. \quad (7)$$

The PCR results presented in **Figure 19(b)** show that the PCR value is greater than 90% from 10.1 to 26 GHz, indicating that most of the energy is converted to its orthogonal counter part in this band. The R_{xx} attains three minimum values at: -49.6 , -54.5 , -45.3 dB, and the corresponding frequencies are 11.1, 17.5, and 25.1 GHz, respectively with a PCR of 100% at 11.1, 17.5, and 25.1 GHz frequencies.

The incident wave with polarization direction along the y -axis is decomposed into u - and v -components to explain the cross polarization conversion mechanism, as illustrated in **Figure 18(b)**. The u - and v components are mutually orthogonal and

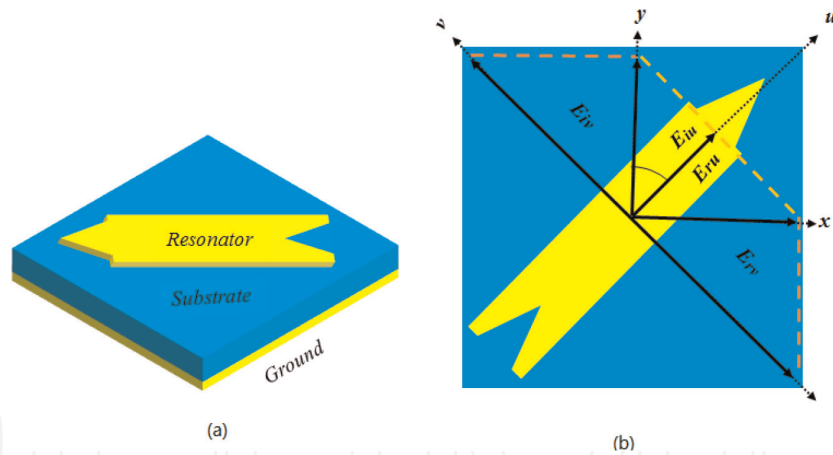


Figure 18. The designed PCMS: (a) unit cell, and (b) $u - v$ decomposition.

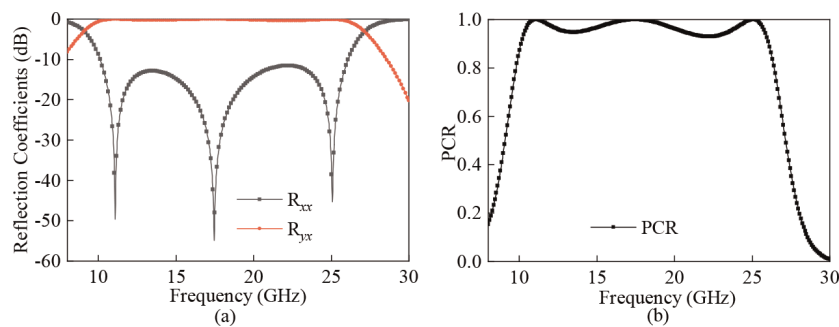


Figure 19. Simulated reflection coefficients of LP waves: (a) x , and (b) PCR of the proposed metasurface.

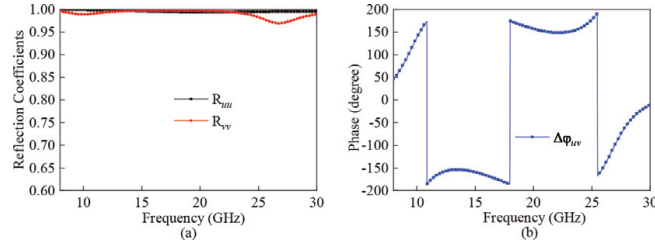


Figure 20. Simulated reflection coefficients: (a) u and v , and (b) Phase difference.

form a $\pm 45^\circ$ angle with the y -axis. The y -polarized incident electric field \vec{E}_i , along the u - and v -axis is expressed as:

$$\vec{E}_i = \hat{u}E_{iu}e^{j\phi} + \hat{v}E_{iv}e^{j\phi} \quad (8)$$

where \hat{u} and \hat{v} are the unit vectors, and φ is the phase of the components. The x -polarized reflected electric field, i.e., \vec{E}_r , can be expressed as:

$$\vec{E}_r = \hat{u}E_{ru}e^{j\phi} + \hat{v}E_{rv}e^{j(\phi \pm 180^\circ)}, \quad (9)$$

where $\varphi = \varphi_{uu}$ and $\varphi \pm 180^\circ = \varphi_{vv}$. The co-polarized reflection coefficients along the u - and v -axes are $r_{uu} = E_u^{\text{ref}}/E_u^{\text{inc}}$ and $r_{vv} = E_v^{\text{ref}}/E_v^{\text{inc}}$. The reflection amplitudes are ($r_{uu} = r_{vv} = 1$) and the phase difference is ($\Delta\varphi = \varphi_{uu} - \varphi_{vv} = \pm 180^\circ$) for CPC through reflected wave in the u - and v -direction [54].

The unit cell was simulated to polarized incidences in the u - and v directions to test the CPC. The results are shown in **Figure 20**. **Figure 20(a)** shows that the amplitudes of the co-polarized coefficients r_{uu} and r_{vv} are close to unity. **Figure 20(b)** shows that in the frequency range (10.1–26 GHz), the phase difference between the u - and v -axis components does not vary much over 180° , validating the effectiveness of cross polarization conversion.

For reflection type of PCMS, the surface currents on both top and bottom surfaces are found to be diagonal. As a result, the field components along the original incident direction are canceled whereas the other one is enhanced in the mutual orthogonal direction. Because the induced field is oriented in an orthogonal direction, it can produce a perpendicularly oriented electric field to the incident one, resulting in polarization conversion of EM waves [55].

The principle of CPC is further explained by the surface current distributions shown in **Figure 21**. At resonance frequencies of 11.1 and 17.6 GHz, the surface currents on the patch and ground are anti parallel resulting in magnetic resonance. At resonance frequency if 25.1 GHz, the surface currents on the patch and ground are parallel resulting in electric resonance. The occurrence of electric and magnetic resonances results in wideband polarization conversion with a high PCR.

4.2 Metasurfaces for radar cross section reduction

Radar cross section (RCS), an essential property of a radar, is a measure of how detectable an object is by radar. The larger the RCS, the easier it is for the object to be detected. A unit cell and its mirror are required for the RCS reduction using polarization converting technique. The unit cell and its mirror unit cell has a cross polarization

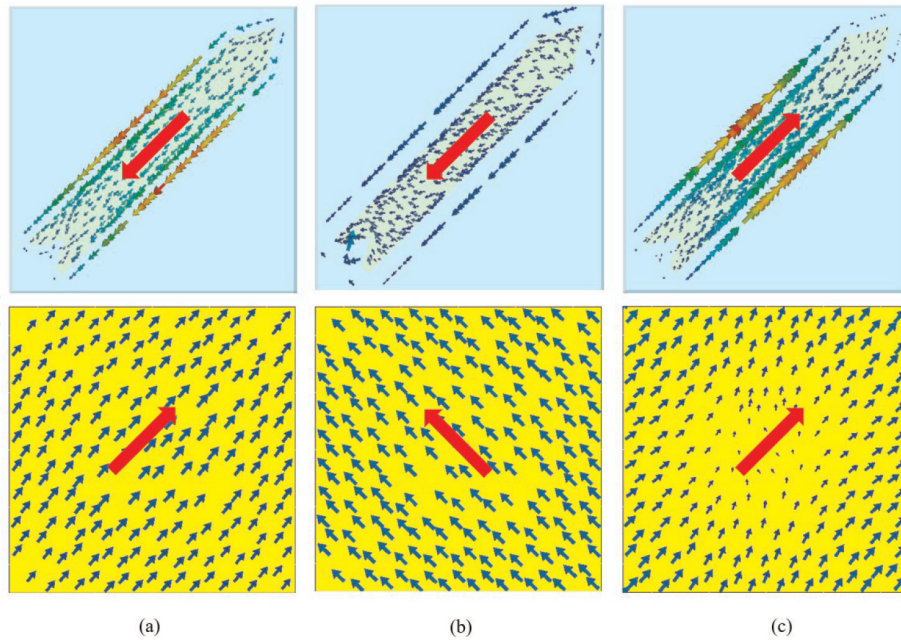


Figure 21.
 Surface current distribution of the top metal and ground metal at resonant eigen-modes: (a) 11.1 GHz, (b) 17.6 GHz, and (c) 25.1 GHz.

phase difference of 180° , which fully satisfies the requirement for RCS reduction. For RCS reduction, chessboard structures are utilized that usually use single PCMS unit and its mirror unit (rotating the same structure by 90°). As per the polarization conversion concept, the phase difference between the PCMS and its mirror should always be 180° . As a result, the PCR is the only component that influences RCS reduction performance. So, when an x -polarized incident waves is reflected, it totally changes to an orthogonal counterpart. The PCMS units reflections, as well as their mirror reflections, are canceled out. As a result, by arranging PCMS units and their mirrors in chessboard structures, the RCS can be minimized.

Figure 22(a) shows the reflection coefficients of the mirror PCMS, which are the same as the reflection coefficients of PCMS. **Figure 22(b)** plots the phase difference between the reflection phases of PCMS and its mirror PCMS unit cells. In the whole PCR bandwidth, there is a 180° reflection phase difference between PCMS and its mirrored PCMS unit cell, indicating that the proposed PCMS satisfies the reflection

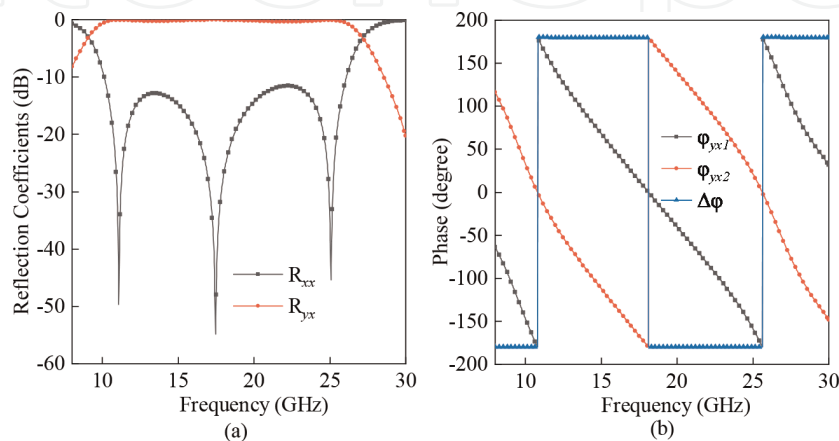


Figure 22.
 Simulated results of: (a) reflection coefficients of mirror PCM, and (b) reflection phase of PCM and its mirror.

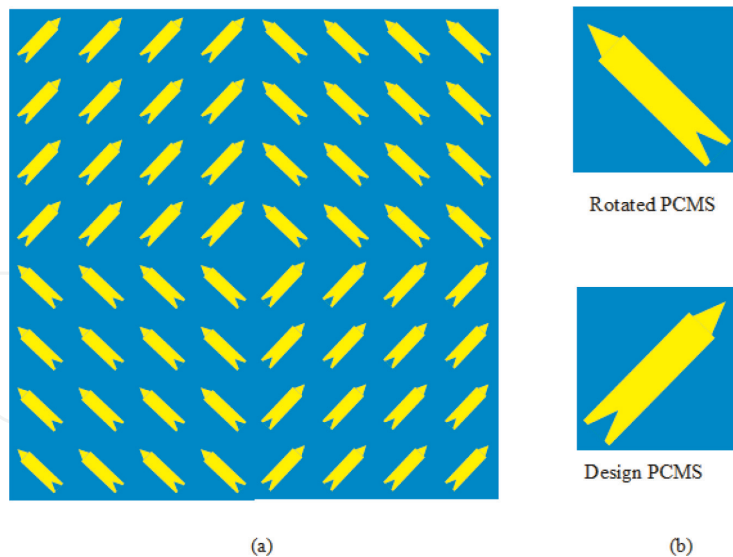


Figure 23.
Top view of the designed square chessboard array with PCMS and its mirror.

phase cancellation requirements for RCS reduction. The RCS reduction from the surface compared to the PEC can be expressed as [56]

$$\begin{aligned} \text{RCS reduction (dB)} &= 10 \log_{10} \left[\frac{\lim_{r \rightarrow \infty} 4\pi r^2 \frac{|\vec{E}_{rx}|^2}{|\vec{E}_{ix}|^2}}{\lim_{r \rightarrow \infty} 4\pi r^2 |1|^2} \right] \\ &= R_{xx} \text{ (dB)} = 10 \log_{10}(1 - \text{PCR}), \end{aligned} \quad (10)$$

where $|E_{rx}|$ and $|E_{ix}|$ are the reflected and incident fields in the far zone of $r \rightarrow \infty$, respectively, r is the detecting distance, and R_{xx} represents the co-polarized reflection coefficients [56]. According to the above equation, RCS reduction is related to PCR. The bandwidth of RCS reduction is predicted from bandwidth of PCR. If PCR is greater than 90%, a 10-dB RCS reduction is achieved.

Based on the designed PCMS unit, an array with 8×8 units and a total dimension of 56×56 was designed in square chessboard configuration as shown in **Figure 23**. The designed PCMS is rotated at an angle of 90° , 180° , and 270° to make a square chessboard configuration, which reflects the wave in-phase and out-phase to create destructive interference, resulting in RCS reduction. The comparison of the proposed square chessboard array monostatic RCS performance with a PEC of the same dimension is shown in **Figure 24**. The designed square chessboard array achieved ultra-wideband RCS reduction in a frequency band from 9.6 to 27.5 GHz. The RCS reduction is maximum at the resonance frequencies of 10.3, 11.8, 19.8, and 20.3 GHz, with the maximum RCS reduction of 27.8 dB observed at 10.3 GHz.

4.3 Metasurfaces for absorption

Metasurfaces can also be utilized for designing perfect absorbers, which absorb most energy of the incident EM wave within the desired frequency band. Metasurface structures with symmetric resonators have been used as effective absorbers with low

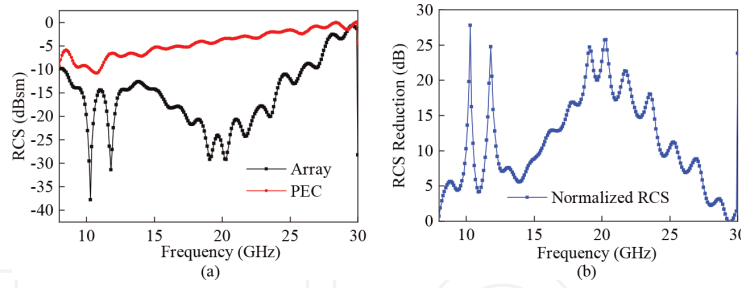


Figure 24. Mono-static RCS reduction: (a) PCMS and PEC, and (b) normalized RCS.

co- and cross polarization reflection [57]. Metasurface absorbers (MSAs) usually consists of subwavelength resonant metal insulator metal (MIM) structures. Mathematically, the absorption can be expressed by the following equation

$$A(\omega) = 1 - R(\omega) - T(\omega), \quad (11)$$

where

$$R(\omega) = \frac{Z_\omega - Z_o}{Z_\omega + Z_o}, \quad (12)$$

$$Z(\omega) = \sqrt{\frac{\mu_o \mu_r(\omega)}{\epsilon_o \epsilon_r(\omega)}}, \quad (13)$$

$$Z_o = \sqrt{\frac{\mu(\omega)}{\epsilon(\omega)}}, \quad (14)$$

with Z_o being the characteristic impedance of the free space, which is equal to 377Ω . The free space permeability and permittivity are denoted by μ_o , and ϵ_o , and μ_r , ϵ_r represents the relative permeability and permittivity in the material. To design an MSA, the unit cell's parameters should be precisely adjusted such that the absorbers impedance matches the free space impedance so the reflection is minimized, resulting in perfect absorption of the incident waves. The effective impedance of the MSA matches the free space impedance by altering the electric and magnetic resonance simultaneously. Metasurface absorbers are characterized by unit cells having single and multi resonant designs, transforming into narrowband and broadband absorption, respectively [58]. In general, the resonance frequency of the MSA is determined by the geometric configuration and geometric characteristics of a unit cell. Metasurface based absorbers are low profile, light weight, with simple metallic structures. They have limitations in terms of absorption bandwidth, absorption rate and air breakdown at high power [59]. The bottom side of the metasurface absorber is a metallic sheet. It acts as a ground, which causes no transmission and consequently $T(\omega)$ is equal to zero. Absorption can also be defined as:

$$A(\omega) = 1 - |R_{xx}|^2 - |R_{yx}|^2 - T, \quad (15)$$

where $|R_{xx}|^2$ and $|R_{yx}|^2$ represents the co- and cross-polarized reflected powers, the transmitted power, i.e., T , is zero because of the metallic ground plane. For absorption

both components of the reflected wave, i.e., co and cross should be zero. A metasurface absorber is designed using square ring resonator made of copper placed at the top of dielectric substrate FR-4 having metallic ground plane on the back side as shown in **Figure 25**. The plots of reflection coefficients and absorption are shown in **Figure 26**. For perfect absorption, the levels of both the co- and cross components of the reflection coefficients should be smaller than -10 dB, i.e., $|R_{xx}|, |R_{yx}| < -10$ dB. The results shown in **Figure 26(a)** indicates that both the co- and cross components of the reflection coefficients are below -10 dB, which indicates that all of the incident wave is absorbed. The results in **Figure 26(b)** show that absorption remains above 90%, which is requirement for perfect absorption.

The intrinsic parameters of the metasurface, i.e., effective permittivity (ϵ_{eff}), effective permeability (μ_{eff}), and effective impedance (z), are obtained by S-parameter-retrieval method [60, 61]. These parameters are extracted as:

$$z = \pm \sqrt{\frac{(1 + S_{11})^2 - S_{21}^2}{(1 + S_{11})^2 - S_{21}^2}}, \quad (16)$$

$$e^{jnK_0H} = \frac{S_{21}}{1 - S_{11}\left(\frac{z-1}{z+1}\right)}, \quad (17)$$

$$\epsilon_{\text{eff}} = \frac{n}{z}, \quad (18)$$

$$\mu_{\text{eff}} = n \times z, \quad (19)$$



Figure 25.
Proposed metasurface absorber.

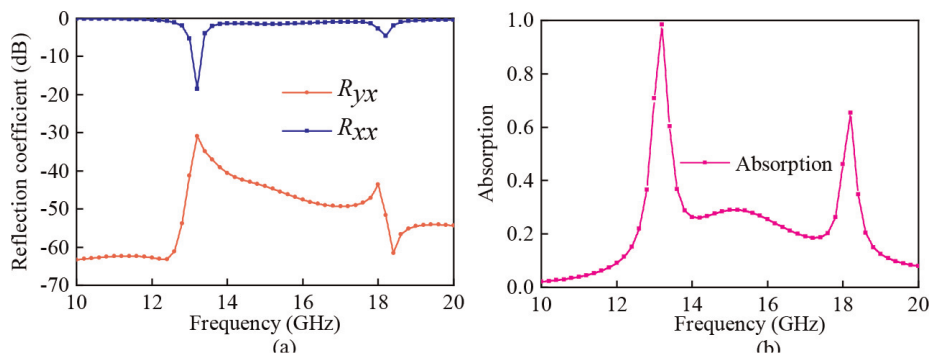


Figure 26.
(a) Reflection coefficients, and (b) absorption.

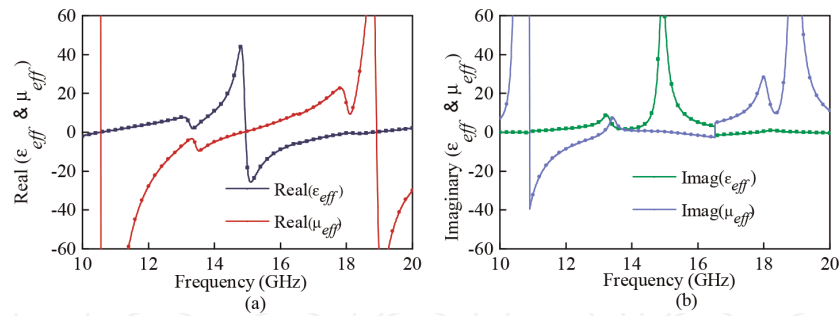


Figure 27.
Extracted effective parameters: (a) real, and (b) imaginary parts.

where z stands for impedance, S_{11} and S_{21} for reflection and transmission amplitudes, n for refractive index, K_o for wave number, and H for substrate thickness [62]. The values of the extracted parameters are shown in **Figure 27**. At peak frequencies of 7.8 and 16.7 GHz, the real and imaginary components of the extracted permittivity, and permeability obtained are almost equal, resulting in impedance matching of the MS with free space, which minimizes the co-polarization reflection and maximizes the absorption [63].

5. Conclusions

This chapter described the applications of metamaterials and metasurfaces. The underlying principles and design considerations of metamaterials in antenna design were explained in detail. The state-of-the-art works related to the application of metamaterials in antenna designs were reviewed. Also it is discussed that how metamaterials are used to improve and enhance the antenna parameters such as gain, directivity, bandwidth, size, and SAR. Moreover, the theoretical concepts and mathematical analysis of metasurfaces for polarization conversion, RCS reduction, and absorption were also discussed. Some metasurfaces were designed to show how to achieve different desired functionalities.

Author details


Babar Kamal^{1*}, Usman Ali², Jingdong Chen¹ and Sadiq Ullah²

1 Center of Intelligent Acoustics and Immersive Communication, School of Marine Science and Technology, Northwestern Polytechnical University, Xian, China

2 University of Engineering and Technology, Mardan, Pakistan

*Address all correspondence to: babarkamal.55@mail.nwpu.edu.cn

IntechOpen

© 2022 The Author(s). Licensee IntechOpen. This chapter is distributed under the terms of the Creative Commons Attribution License (<http://creativecommons.org/licenses/by/3.0>), which permits unrestricted use, distribution, and reproduction in any medium, provided the original work is properly cited. 

References

- [1] Shivola A. Metamaterials in electromagnetics. *Metamaterials*. 2007; **1**(1):2-11. DOI: 10.1016/j.metamat.2007.02.003
- [2] Smith DR, Padilla WJ, Vier DC, Nemat-Nasser SC, Schultz S. Composite medium with simultaneously negative permeability and permittivity. *Physical Review Letters*. 2000;**84**(18):4184. DOI: 10.1103/PhysRevLett.84.4184
- [3] Walia S, Shah CM, Gutruf P, et al. Flexible metasurfaces and metamaterials: A review of materials and fabrication processes at micro-and nano-scales. *Applied Physics Review*. 2015;**2**(1):011303. DOI: 10.1063/1.4913751
- [4] Freire MJ, Marques R, Jelinek L. Experimental demonstration of a $\hat{\mu} = -1$ metamaterial lens for magnetic resonance imaging. *Applied Physics Letters*. 2008;**93**(23):1-4. DOI: 10.1063/1.3043725
- [5] Ozbey B, Demir HV, Kurc O, Erturk VB, Altintas A. Wireless measurement of elastic and plastic deformation by a metamaterial-based sensor. *Sensors*. 2014;**14**(10):19609-19621. DOI: 10.3390/s141019609
- [6] Liu W, Chen ZN, Qing X. Metamaterial-based low-profile broadband mushroom antenna. *IEEE Transactions on Antennas and Propagation*. 2013;**62**(3):1165-1172. DOI: 10.1109/TAP.2013.2293788
- [7] Glybovski SB, Tretyakov SA, Belov PA, Kivshar YS, Simovski CR. Metasurfaces: From microwaves to visible. *Physics Reports*. 2016;**634**:1-72. DOI: 10.1016/j.physrep.2016.04.004
- [8] Holloway CL, Kuester EF, Gordon JA, O'Hara J, Booth J, Smith DR. An overview of the theory and applications of metasurfaces: The two-dimensional equivalents of metamaterials. *IEEE Antennas Propagation Magazines*. 2012; **54**:10-35. DOI: 10.1109/MAP.2012.6230714
- [9] Chen HT, Taylor AJ, Yu N. A review of metasurfaces: Physics and applications. *Reports on Progress in Physics*. 2016;**79**(7):076401. DOI: 10.1088/0034-4885/79/7/076401
- [10] Li F, Chen H, He Q, Zhou Y, Zhang L, Weng X, et al. Design and implementation of metamaterial polarization converter with the reflection and transmission polarization conversion simultaneously. *Journal of Optics*. 2020;**21**(4):04510. DOI: 10.1088/2040-8986/ab0878
- [11] Roy T, Rogers ET, Zheludev NI. Sub-wavelength focusing meta-lens. *Optics Express*. 2013;**21**(6):75777582
- [12] Azad AK et al. Metasurface broadband solar absorber. *Scientific Reports*. 2016;**6**(1):16. DOI: 10.1038/srep20347
- [13] Ni X et al. An ultrathin invisibility skin cloak for visible light. *Science*. 2015; **349**(6254):13101314. DOI: 10.1126/science.aac9411
- [14] Zhang XG et al. A metasurface-based light-to-microwave transmitter for hybrid wireless communication. *Light: Science & Applications*. 2022;**11**(126):1-10. DOI: 10.1038/s41377-022-00817-5
- [15] Khan B, Kamal B, Ullah S, Abdullah AH, Ullah R. Asymmetric polarization converting metasurface for microwave application. *Optical Material Express*. 2022;**12**(9):3403-3415. DOI: 10.1364/OME.455472

- [16] Amiri M, Tofigh F, Shariati N, Lipman J, Abolhasan M. Review on metamaterial perfect absorbers and their applications to IoT. *IEEE Internet of Things Journal*. 2020;**8**(6):4105-4131. DOI: 10.1109/JIOT.2020.3025585
- [17] Miliadis C, Andersen RB, Lazaridis PI, Zaharis ZD, Muhammad B, Kristensen JT, et al. Metamaterial-inspired antennas: A review of the state of the art and future design challenges. *IEEE Access*. 2021;**9**:89846-89865. DOI: 10.1109/ACCESS.2021.3091479
- [18] Ali Esmail B, Majid HA, Zainal Abidin Z, Haimi Dahlan S, Himdi M, Dewan R, et al. Reconfigurable radiation pattern of planar antenna using metamaterial for 5G applications. *Materials*. 2020;**13**(3):582. DOI: 10.3390/ma13030582
- [19] Agarwal S, Prajapati YK. Multifunctional metamaterial surface for absorbing and sensing applications. *Optics Communications*. 2019;**439**:304-307. DOI: 10.1016/j.optcom.2019.01.020
- [20] Tadesse AD, Acharya OP, Sahu S. Application of metamaterials for performance enhancement of planar antennas: A review. *International Journal of RF and Microwave Computer & Aided Engineering*. 2020;**30**(5):e22154. DOI: 10.1002/mmce.22154
- [21] Asif M, Sehrai DA, Kiani SH, Khan J, Abdullah M, Ibrar M, et al. Design of a dual band SNG metamaterial based antenna for LTE 4G/WLAN and Ka-band applications. *IEEE Access*. 2021;**9**:71553-71562. DOI: 10.1109/ACCESS.2021.3077844
- [22] Rosaline SI. A triple-band antenna with a metamaterial slab for gain enhancement and specific absorption rate (SAR) reduction. *Progress in Electromagnetic Research C*. 2021;**109**:275-287. DOI: 10.2528/PIERC20122202
- [23] Ali U, Ullah S, Shafi M, Shah SA, Shah IA, Flint JA. Design and comparative analysis of conventional and metamaterial-based textile antennas for wearable applications. *International Journal of Numerical Modelling: Electronic Networks, Devices and Fields*. 2019;**32**(6):e2567. DOI: 10.1002/jnm.2567
- [24] Yayun D, Wenwen L, Xijun Y, Chen Y, Houjun T. Design of unit cell for metamaterials applied in a wireless power transfer system. In: *IEEE PELS Workshop on Emerging Technologies: Wireless Power Transfer*. 2017. pp. 143-147. DOI: 10.1109/WoW.2017.7959382
- [25] Phan DT, Phan HL, Nguyen TQH. A miniaturization of microstrip antenna using negative permittivity metamaterial based on CSRR loaded ground for WLAN applications. *Journal of Science and Technology*. 2016;**54**(6):689-697. DOI: 10.15625/0866-708X/54/6/8375
- [26] Krzysztofik WJ, Cao TN. Metamaterials in application to improve antenna parameters. *Metamaterials and Metasurfaces*. 2018;**12**(2):63-85
- [27] Ali U, Ullah S, Khan J, Shafi M, Kamal B, Basir A, et al. Design and SAR analysis of wearable antenna on various parts of human body, using conventional and artificial ground planes. *Journal of Electrical Engineering and Technology*. 2017;**12**(1):317-328. DOI: 10.5370/JEET.2017.12.1.317
- [28] Lu G, Yan F, Zhang K, Zhao Y, Zhang L, Shang Z, et al. A dual-band high-gain subwavelength cavity antenna with artificial magnetic conductor metamaterial microstructures. *Micromachines*. 2021;**13**(1):58. DOI: 10.3390/mi13010058

- [29] Gong Y, Yang S, Li B, Chen Y, Tong F, Yu C. Multi-band and high gain antenna using AMC ground characterized with four zero-phases of reflection coefficient. *IEEE Access*. 2020; **8**:171457-171468. DOI: 10.1109/ACCESS.2020.3024982
- [30] Sievenpiper D, Zhang L, Broas RF, Alexopolous NG, Yablonovitch E. High-impedance electromagnetic surfaces with a forbidden frequency band. *IEEE Transactions on Microwave Theory and Techniques*. 1999; **47**(11):2059-2074. DOI: 10.1109/22.798001
- [31] Yanagi T, Oshima T, Oh-hashii H, Konishi Y, Murakami S, Itoh K, et al. Lumped-element loaded EBG structure with an enhanced bandgap and homogeneity. In: 2008 International Workshop on Antenna Technology: Small Antennas and Novel Metamaterials. 2008. pp. 458-461. DOI: 10.1109/IWAT.2008.4511377
- [32] Zheng YJ, Gao J, Zhou YL, Cao XY, Xu LM, Li SJ, et al. Metamaterial based patch antenna with wideband RCS reduction and gain enhancement using improved loading method. *IET Microwaves, Antennas & Propagation*. 2017; **11**(9):1183-1189. DOI: 10.1049/iet-map.2016.0746
- [33] Roy S, Chakraborty U. Metamaterial-embedded dual wideband microstrip antenna for 2.4 GHz WLAN and 8.2 GHz ITU band applications. *Waves in Random and Complex Media*. 2020; **30**(2):193-207. DOI: 10.1080/17455030.2018.1494396
- [34] Sumathi K, Lavadiya S, Yin P, Parmar J, Patel SK. High gain multiband and frequency reconfigurable metamaterial superstrate microstrip patch antenna for C/X/Ku-band wireless network applications. *Wireless Networks*. 2021; **27**(3):2131-2146. DOI: 10.1007
- [35] Jeong H, Kim Y, Tentzeris MM, Lim S. Gain-enhanced metamaterial absorber-loaded monopole antenna for reduced radar cross-section and back radiation. *Materials*. 2020; **13**(5):1247. DOI: 10.3390/ma13051247
- [36] Bakhtiari A, Sadeghzadeh RA, Moghadasi MN. Gain enhanced miniaturized microstrip patch antenna using metamaterial superstrates. *IETE Journal of Research*; **65**(5):635-640. DOI: 10.1080/03772063.2018.1447406
- [37] Gao XJ, Cai T, Zhu L. Enhancement of gain and directivity for microstrip antenna using negative permeability metamaterial. *AEU-International Journal of Electronics and Communications*. 2016; **70**(7):880-885. DOI: 10.1016/j.aeue.2016.03.019
- [38] Khoutar FZ, Aznabet M, Mrabet OEL, Nayat-Ali O. Double layer metamaterial superstrate for performance enhancement of a microstrip patch antenna. In: ICCWCS 2019: Third International Conference on Computing and Wireless Communication Systems, ICCWCS 2019, April 24-25, Faculty of Sciences, Ibn Tofal University-Knitra-Morocco, 82. European Alliance for Innovation DOI: 10.4108/eai.24-4-2019.2284232
- [39] Al-Bawri SS, Islam MS, Wong HY, Jamlos MF, Narbudowicz A, Jusoh M, et al. Metamaterial cell-based superstrate towards bandwidth and gain enhancement of quad-band CPW-fed antenna for wireless applications. *Sensors*. 2020; **20**(2):457. DOI: 10.3390/s20020457
- [40] Raval F, Kosta YP, Joshi H. Reduced size patch antenna using complementary split ring resonator as defected ground

plane. *AEU-International Journal of Electronics and Communications*. 2015; **69**(8):1126-1133. DOI: 10.1016/j.aeue.2015.04.013

[41] Varamini G, Keshtkar A, Naser-Moghadasi M. Miniaturization of microstrip loop antenna for wireless applications based on metamaterial metasurface. *AEU-International Journal of Electronics and Communications*. 2018;**83**:32-39. DOI: 10.1016/j.aeue.2017.08.024

[42] Hediya AM. Reduction of specific absorption rate: A review article. *The Egyptian International Journal of Engineering Sciences and Technology*. 2022. DOI: 10.21608/eijest.2022.108455.1117

[43] Karimian R, Ardakani MD, Ahmadi S, Zaghloul M. Human body specific absorption rate reduction employing a compact magneto-dielectric AMC structure for 5G massive-MIMO applications. *Engineering*. 2021;**2**(4): 501-511. DOI: 10.3390/eng2040032

[44] Haridim M. Use of rod reflectors for SAR reduction in human head. *IEEE Transactions on Electromagnetic Compatibility*. 2015;**58**(1):40-46. DOI: 10.1109/TEMC.2015.2500818

[45] Stephen JP, Hemanth DJ. An investigation on specific absorption rate reduction materials with human tissue cube for biomedical applications. *International Journal of RF and Microwave Computer Aided Engineering*. 2019;**29**(12):e21960. DOI: 10.1002/mmce.21960

[46] Pikale R, Sangani D, Chaturvedi P, Soni A, Munde M. A review: Methods to lower specific absorption rate for mobile phones. In: 2018 International Conference On Advances in Communication and Computing

Technology (ICACCT). IEEE. 2018. pp. 340-343. DOI: 10.1109/ICACCT.2018.8529654

[47] Sugumaran B, Balasubramanian R, Palaniswamy SK. Reduced specific absorption rate compact flexible monopole antenna system for smart wearable wireless communications. *Engineering Science and Technology, an International Journal*. 2021;**24**(3):682-693. DOI: 10.1016/j.jestch.2020.12.012

[48] Imaculate Rosaline S, Raghavan S. Design and analysis of a SRR superstrate for SAR reduction. *Journal of Electromagnetic Waves and Applications*. 2015;**29**(17):2330-2338. DOI: 10.1080/09205071.2015.1091384

[49] Tamim AM, Faruque MRI, Khandaker MU, Islam MT, Bradley DA. Electromagnetic radiation reduction using novel metamaterial for cellular applications. *Radiation Physics and Chemistry*. 2021;**178**:108976. DOI: 10.1016/j.radphyschem.2020.108976

[50] Tayaalen R, Mohammad RIF, Mohammad TI. Specific absorption rate reduction for sub-6 frequency range using polarization dependent metamaterial with high effective medium ratio. *Scientific Reports*. 2022;**12**(1):1-18. DOI: DOI; 10.1007/s11664-019-07156-z

[51] Ashyap AY, Zainal Abidin Z, Dahlan SH, Majid HA, Saleh G. Metamaterial inspired fabric antenna for wearable applications. *International Journal of RF and Microwave Computer Aided Engineering*. 2019;**29**(3):e21640. DOI: 10.1002/mmce.21640

[52] Kamal B, Chen J, Yin Y, Ren J, Ullah S, Khan B. Broad band and broad angle linear and circular polarization converting metasurface. *Journal of Electromagnetic Waves and*

Applications. 2022;**36**(8):1102-1112.
DOI: 10.1080/09205071.2021.2005696

Nano. 2018;**7**(6):989-1011. DOI: 10.1515/
nanoph-2017-0120

[53] Kamal B, Chen J, Yin Y, Ren J, Ullah S, Ali U. Design and experimental analysis of dual-band polarization converting metasurface. *IEEE Antennas and Wireless Propagation Letters*. 2021;**20**(8):1409-1413. DOI: 10.1109/LAWP.2021.3083334

[60] Smith D, Schultz S, Markois P, Soukoulis C. Determination of effective permittivity and permeability of metamaterials from reflection and transmission coefficients. *Physical Review B*. 2002;**65**(19):195104. DOI: 10.1103/PhysRevB.65.195104

[54] Abdullah KB, Ullah S, Khan B, Ali H, Rahim T. Cross polarization conversion metasurface for fixed wireless and ku-band applications. *International Journal of Communication Systems*. 2022;**35**(3):e5033. DOI: 10.1002/dac.5033

[61] Numan AB, Sharawi MS. Extraction of material parameters for metamaterials using a full-wave simulator [education column]. *IEEE Antennas and Propagation Magazine*. 2013;**55**(5):202-211. DOI: 10.1109/MAP.2013.6735515

[55] Bhattacharya S, Saha C, Siddiqui and JY. High frequency applications of metamaterials and metasurfaces. In: *Proceedings of the IEEE Recent Advances in Geoscience and Remote Sensing: Technologies, Standards and Applications (TENGARSS'19)*; 17-20 October 2019; Kochi, India IEEE. 2019. pp. 96-99

[62] Khan B, Kamal B, Ullah S, Khan I, Shah JA, Chen J. Design and experimental analysis of dual-band polarization converting metasurface for microwave applications. *Scientific Reports*. 2020;**10**(1):1-13. DOI: 10.1038/s41598-020-71959-y

[56] Fu C, Han L, Liu C, Sun Z, Lu X. Dual-band polarization conversion metasurface for RCS reduction. *IEEE Transactions on Antennas and Propagation*. 2020;**69**(5):3044-3049. DOI: 10.1109/TAP.2020.3028148

[63] Abdullah KB, Ullah S, Khan B, Rahim T, Ren J. Ultrathin and high efficient wideband polarization converting metasurface. *International Journal of RF and Microwave Computer-Aided Engineering*. 2021;**31**(7):e22673. DOI: 10.1002/mmce.22673

[57] Kamal B, Chen J, Yin Y, Ren J, Ullah S, Khan WUR. High efficiency and ultrawideband polarization converter based on L-shaped metasurface. *Optical Material Express*. 2021;**5**(1):1343-1352. DOI: 10.1034/OME.423324

[58] Ding F, Pors A, Bozhevolnyi SI. Gradient metasurfaces: A review of fundamentals and applications. *Reports on Progress in Physics*. 2018;**81**(2):026401. DOI: 10.1088/1361-6633/aaa8732

[59] Li A, Singh S, Sievenpiper D. *Metasurfaces and their applications*.